Superconductor superlattice model for small-angle grain boundaries in Y-Ba-Cu-O

D. Agassi
Naval Surface Warfare Center, White Oak, Maryland 20903

C. S. Pande and R. A. Masumura
Naval Research Laboratory, Washington D.C. 20375

(Received 23 November 1994; revised manuscript received 10 May 1995)

The measured critical current ratios of small-angle Y-Ba-Cu-O grain boundaries fabricated by Dimos *et al.*, are calculated from a superconducting superlattice model where the periodicity is given by the Read-Shockley formula. The layers' thicknesses are estimated from stress-field calculations of a periodic edge-dislocations array model. The measured critical current dependence on the misalignment angle and the temperature are reproduced with a single fitting parameter. This parameter is related to the stress field in proximity to an edge dislocation. The model's validity and comparison with other attempts at the same data are discussed.

I. INTRODUCTION

Shortly after the discovery of high-temperature superconductors (HTS's) it was realized that grain boundaries (GB's) in some HTS ceramics suppress the critical current (j_c).[1] In a pioneering series of experiments aimed at identifying the factors responsible for such a "weak-link" GB behavior, Dimos *et al.* fabricated a particular, controlled, GB structure:[2] Growing a thin epitaxial [001] (and [001]) Y-Ba-Cu-O film on a $SrTiO_3$ bycrystal substrate with a prescribed misalignment angle θ of the two subcrystals ($\theta=0$ corresponds to a single crystal), the film assumes the substrate's configuration. The slab-shaped domain where the two Y-Ba-Cu-O subcrystals mesh is surmised to represent a GB in ceramics. The measured critical current density, hereafter denoted by j_c, in the direction normal to the GB plane and at $T=4.2$ K, shows a sharp exponential drop with rising θ for $\theta\lesssim 8°$, followed by a small-j_c plateau for the higher θ range.[2(b)] This result implies that an almost-perfect grain alignment is necessary for achieving high j_c in HTS ceramics.[2(b),2(c)] Other studies[2(c)] show a characteristic falloff of j_c ($\theta=5°$, T) as the temperature increases.

The difference in the measured j_c ($\theta, T=4.2$ K) behavior for small and large θ correlates with the difference in the corresponding GB structures. Transmission electron microscopy (TEM) studies of the small-angle GB's [Refs. 2(b), 3] reveal a structure comprised of an ordered array of isolated edge dislocations, Fig. 1(a), with spacing d conforming to the Read-Shockley formula[4]

$$d=\frac{b}{\sin\theta}, \tag{1.1}$$

where b is the corresponding Burgers vector. For the [001] GB's, which are the only ones modeled in this work, the analysis gives $b=3.8$ Å.[2(b),3] As (1.1) implies, the spacing between dislocations shrinks with increasing θ to the point where they coalesce to form a continuous slab. Provided this slab acts as a tunneling barrier, such a GB may be characterized as a Josephson junction, in keeping with large-angle GB data.[2(c)]

It should be emphasized that GB's in other systems, such as in flux-melt ceramics and sputtered thin films, have transport properties which are probably controlled by factors other than the misalignment angle.[5,6] In particular, the level of local oxygenation correlates with current transport properties of "nonweak" GB's.[5,7] The interplay of these and other possible material-specific factors in determining the j_c associated with a particular type of GB is still the subject of active research.

In this work we propose a phenomenological model for the j_c data of the small-angle GB's fabricated by Dimos *et al.*[2] This type of GB is modeled as a S-S' superconductor superlattice, where the edge-dislocation cores and the host superconductor material between the cores are represented by "bad" and "good" superconducting slabs, respectively: see Fig. 1(c). We arrive at this model by the following reasoning. The small-angle GB structure, i.e., a periodic array of edge dislocations,[2(b),3] Fig. 1(a), implies the presence of an associated periodic, geometrically complex stress field. Our first premise is that the "highly" stressed domains around the dislocation centers—with either positive or negative stress—constitute a degraded superconducting phase of the host superconductor. This premise is based on indications that local stress in proximity to an extended defect enhances local outdiffusion of the volatile oxygen atoms through the defect.[7] The corresponding deoxygenation in HTS's implies a well-known degradation of T_c. By the same token, the material outside the highly stressed domains constitutes the host HTS material. Consequently, the GB's under discussion constitute a periodic configuration of geometrically complex superconducting regions, where the periodicity is given by (1.1) and in which the degree of T_c degradation varies continuously.

To simplify the analysis of such a complex configuration, the continuum of T_c degradations is approximated by just two phases, hereafter referred to as the "good" (S) and "bad" (S') superconductor phases, which correspond to the highly and low stressed domains. This is schematically plotted in Fig. 1(b) for a choice of a circular geometry of the highly stressed domains around each edge dislocation. The important issue of demarkation between the high and low stress domains is modeled separately and discussed in the

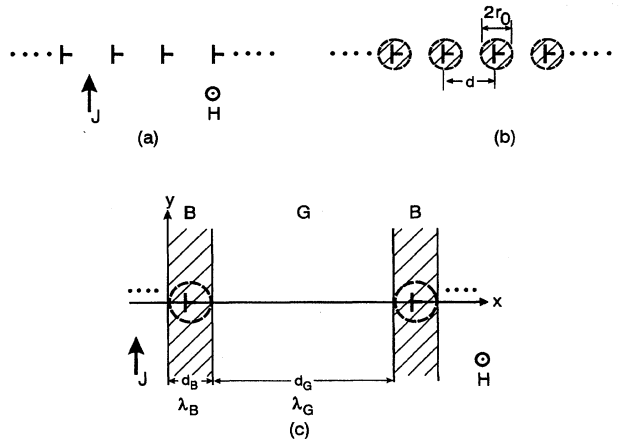

FIG. 1. Schematic depiction of small-angle grain boundary structure and models. (a) The periodic edge-dislocation array observed in TEM studies (Ref. 3). The current (J) and vortices (H) directions normal and parallel to the grain boundary plane, respectively, are indicated. (b) Periodic edge-dislocation array model employed in the calculation of Appendix C. The circular hatched domains, enclosing an edge-dislocation symbol, are assumed to be "highly" strained. The complementary area represents the "low" strain domain. (c) The superconductor-superlattice model employed in the text. The B and G layers designate the "bad" and "good" superconductor layers, respectively, and are characterized by penetration depths λ_B and λ_G, and thicknesses d_B and d_G, respectively. The circular domain enclosing an edge-dislocation symbol in the B layers is a reminder that these layers represent the immediate proximity of the edge-dislocations of (a) and (b). The coordinate system here is the one used in the text.

last section. Furthermore, the complex geometry of the high-low GB stress field, schematically depicted in Fig. 1(b) by circles around the edge dislocations, is drastically simplified by adopting the superlattice geometry of Fig. 1(c), where the superlattice periodicity is still given by (1.1). The good fit to the data in Fig. 4, below, in terms of a single parameter indicates that the superlattice model captures the essential physics of the problem at hand. This legitimacy of this simplification is further discussed in the last section.

The paper is organized as follows: The superconductor superlattice model and the ensuing j_c are analytically evaluated in Sec. II. The results, discussion, and comparison with competing models are given in the last section. Some details of the calculations are given in the Appendixes.

II. MODEL

Since the penetration depth in HTS's is considerably larger than the coherence length, the London limit is valid. In that limit and coordinate system defined in Fig. 1(c), the basic equation for a S-S' superlattice with periodic, piecewise-constant penetration depth $\lambda(x)$, in the presence of a vortex at (x_0,y_0) parallel to the crystal c axis, is the London equation[8]

$$B-\lambda^2(x)\left[\frac{\partial^2}{\partial x^2}+\frac{\partial^2}{\partial y^2}\right]B=\Phi_0\delta(x-x_0)\,\delta(y-y_0), \tag{2.1}$$

where $B(x,y;x_0,y_0)$ is the magnetic field in the c-axis direction and $\Phi_0=\pi\hbar c/|e|=1630$ (eV Å)$^{1/2}$ is the flux quantum. For interfaces at planes $x=x_I$, as in Fig. 1(c), the corresponding boundary conditions are

$$\Delta\left[\lambda^2\left(\frac{\partial B}{\partial x}\right)\right]_{x=x_I}=0, \quad \Delta[B]_{x=x_I}=0, \tag{2.2}$$

where the notation $\Delta\psi(x_I,y)=\psi(x_I+\epsilon,y)-\psi(x_I-\epsilon,y)$ for $\epsilon\to 0$ is employed.

To solve (2.1) we use the Fourier transform method: In each of the two superlattice domains, the homogeneous equation solutions have the representation

$$B_X(x,y)=\int_{-\infty}^{\infty}dk_y e^{ik_y y}B_X(k_y;x), \quad X=G,B, \tag{2.3}$$

where hereafter the G and B labels refer to the "good" and "bad" superconductor superlattice domains. The ensuing equation for $B_X(k_y;x)$, a fixed k_y and a periodic $\lambda^2(x)$, has the structure of a "wave equation" with a periodic "potential." According to the Bloch theorem,[9] its solutions satisfy

$$B_X(k_y;x+d)=e^{-\mu d}B_X(k_y;x), \quad X=G,B, \tag{2.4}$$

where the modulation μ is analogous to the crystal momentum in infinite periodic solids. However, unlike the situation for infinite periodic solids, the boundary condition here is that the solution vanishes at infinity, reflecting the fact that the magnetic field emanating from a vortex decays at a large distance from its location.[10]

Matching the boundary conditions (2.2) for (2.3) yields the key dispersion relation

$$\cosh[\mu d]=\cosh[D_G(k_y)d_G]\cosh[D_B(k_y)d_B]+\left[\frac{1+R^2(k_y)}{2R(k_y)}\right]\sinh[D_G(k_y)d_G]\sinh[D_B(k_y)d_B], \tag{2.5}$$

where

$$R(k_y)=\frac{\lambda_G^2 D_G(k_y)}{\lambda_B^2 D_B(k_y)}, \quad D_X(k_y)=\sqrt{k_y^2+\frac{1}{\lambda_X^2}}, \quad X=G,B, \tag{2.6}$$

and λ_X denotes the constant penetration depth in domain X, Fig. 1(c). Note that (2.5) is invariant under interchange of the B- and G-domain entries. This symmetry is expected since μ, which pertains to the entire superlattice, should not depend on the particular coordinates choice of Fig. 1(c). Also, (2.5) resembles the dispersion relation of the Kronig Penney model[11] with the

important difference that no forbidden k_y domains (or energy gaps) are implied. This feature reflects the elliptic characteristic of (2.1), in distinction to the hyperbolic characteristic of the Schrodinger wave equation.

For a fixed k_y, Eq. (2.5) has two solutions of the form $\pm|\mu|$. The corresponding solutions (2.3) constitute a complete solutions set of the homogeneous equation, from which the solution of (2.1) is constructed following the standard method.[12] Further details are given in Appendix A. The ensuing B-domain pinning potential per unit vortex length L, denoted here by $U_B(x_0)/L$, is[8]

$$\frac{U_B(x_0)}{L}=\frac{\Phi_0^2}{32\pi^2\lambda_B^2}\int_{-\infty}^{\infty}dk_y\,\frac{1}{D_B[1-\beta_B^{(+)}(\mu<)\beta_B^{(-)}(\mu>)]}$$
$$\times[2\beta_B^{(+)}(\mu<)\beta_B^{(-)}(\mu>)+e^{-2D_Bx_0}\beta_B^{(+)}(\mu<)+e^{2D_Bx_0}\beta_B^{(-)}(\mu>)], \tag{2.7a}$$

where $0\leq x_0\leq d_B$ and the β functions are defined by Eq. (A3):

$$\beta_B^{(-)}(k_y,\mu)\equiv\beta_B^{(-)}(\mu)=-\frac{e^{\mu d-D_Bd_B}\left[\frac{(1-R^2)}{2R}\right]\sinh(D_Gd_G)}{1-e^{\mu d+D_Bd_B}\left[\cosh(D_Gd_G)+\left[\frac{(1+R^2)}{2R}\right]\sinh(D_Gd_G)\right]},$$
$$\beta_B^{(+)}(k_y,\mu)\equiv\beta_B^{(+)}(\mu)=\frac{e^{\mu d+D_Bd_B}\left[\frac{(1-R^2)}{2R}\right]\sinh(D_Gd_G)}{1-e^{\mu d-D_Bd_B}\left[\cosh(D_Gd_G)-\left[\frac{(1+R^2)}{2R}\right]\sinh(D_Gd_G)\right]}. \tag{2.7b}$$

In (2.7a), the symbol $\beta_B^{(+)}(\mu<)$, for example, is an abbreviated notation for $\beta_B^{(+)}(k_y,\mu)$, Eq. (2.7b), evaluated with the $\mu<0$ solution of (2.5). All k_y dependences in (2.7) have been suppressed for the sake of notational clarity. The corresponding expressions for the G domain are obtained by interchanging the G- and B-domain entries in (2.7). Together with (2.7), these expressions comprise the exact pinning potential of the superconductor superlattice model in the London limit. Note that the pinning potential does not depend on the y_0 coordinate, reflecting the superlattice translational invariance in the y coordinate.

An example of the calculated pinning potential (2.7) is given in Fig. 2. Plotted is the *total* free energy[8] F_T/L, which is the sum of the pinning potential (2.7) and the vortex self-energy $F_X^{(\mathrm{vor})}/L\approx[\Phi_0/(4\pi\lambda_X)]^2K_0(\xi/\lambda_X)$, where $X=B,G$ and $K_0(z)$ is the modified Bessel function of zeroth order.[13] As expected, the bad domain free energy is lower than that of the good domain, in addition to the characteristic narrow minimum at S-S' interfaces. Note that the minimum and maximum points are at domain midpoints, with concave and convex curvatures, respectively. This particular location of the extrema follows since the infinite superlattice is symmetric to the left and right of each such midpoint. The opposite pinning potential curvatures at the two domains is in keeping with the overall decrease of the free energy with moving from a good to the adjacent bad domain. Therefore, ignoring the interface minima, the maximum *pinning barrier*—associated with the critical current—is the difference of the pinning potentials evaluated at the domain's midpoints.

To identify the controlling parameters in (2.7) and evaluate the critical current, it is instructive to introduce analytic approximations for the relevant case when x_0 in (2.7) is at domain midpoint. The approximations are based on expressions (2.7) evaluated in the physically interesting regime when d_B/λ_B, $d_G/\lambda_G\ll 1$ and $\lambda_G/\lambda_B\ll 1$. Details are given in Appendix B. The focus on this regime is motivated by the sizes of the dislocation cores and spacings, which are small in comparison to typical penetration depths [O(1000 Å)], and the premise that the bad domain is a substantially degraded phase of the good domain. The exact [Eq. (2.7)] and approximate integrands derived in Appendix B are compared in Fig. 3 for a characteristic example. As Fig. 3 shows, the approximation is excellent. The ensuing pinning potentials, Eq. (2.7a), and its G-domain counterpart assume the simple form

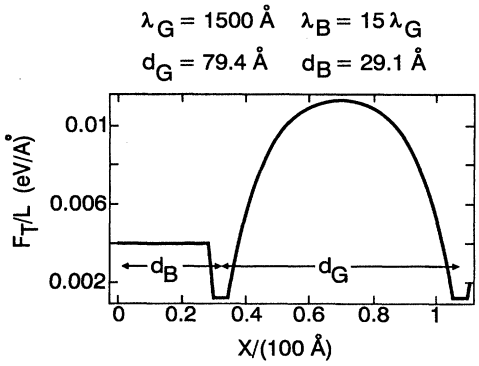

FIG. 2. Calculation of the total free energy per vortex unit length, denoted by F_T/L, in the superlattice unit cell, for the example specified in the header. Indicated are the "good" (d_G) and "bad" (d_B) domains, employing the coordinates of Fig. 1(c). The narrow wells separating the bad and good domains reflect standard cutoffs (Ref. 8) with $\xi=15$ Å.

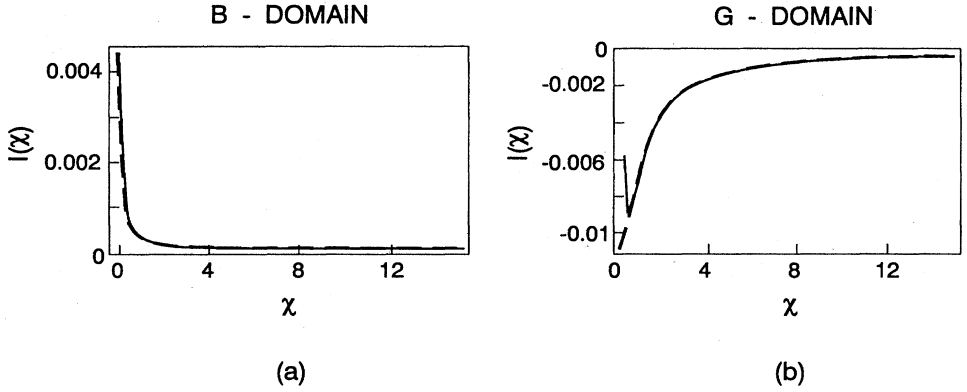

FIG. 3. Comparisons of exact (solid line) and approximated (dashed line) pinning potential integrand $I(\chi)$ for the example: $\lambda_G=1500$ Å, $\lambda_B=3\lambda_G$, $d_G=49.1$ Å, $d_B=174.3$ Å. The abscissa is $\chi=x/\lambda_G$. The exact integral in the B layer is given in Eq. (2.7); the corresponding G layer integral is not quoted in the text. The approximate expressions are derived in Appendix B. (a) In the B domain. (b) In the G domain.

$$\frac{U_G(x_{\rm mid})}{L}\approx-\left(\frac{\Phi_0}{4\pi\lambda_G}\right)^2 K_0\left(\frac{d_G}{\lambda_G}\right),$$

$$\frac{U_B(x_{\rm mid})}{L}\approx 4\left(\frac{\Phi_0}{4\pi\lambda_B}\right)^2 K_0\left(\frac{d_B}{\lambda_B}\right), \tag{2.8}$$

where $x_{\rm mid}$ denotes the midpoint of the pertaining G or B domain. Note that in (2.8) the complicated coupling between the domain [Eq. (2.7)] is absent. The asymmetric form of (2.8) between the B and G domains is discussed in Appendix B.

The critical current j_c is commonly equated to ratio of the maximum *pinning barrier* over a characteristic range.[8] Consequently, employing (2.8) and adding the vortex self-free-energy mentioned above, yields for the measured critical currents the ratio[2]

$$\frac{j_c(\theta)}{j_c(\theta_0)}=\left|\frac{\frac{1}{\lambda_B^2}[K_0(\xi/\lambda_B)+4K_0(d_B(\theta)/\lambda_B)]-\frac{1}{\lambda_G^2}[K_0(\xi/\lambda_G)-K_0(d_G(\theta)/\lambda_G)]}{\frac{1}{\lambda_B^2}[K_0(\xi/\lambda_B)+4K_0(d_B(\theta_0)/\lambda_B)]-\frac{1}{\lambda_G^2}[K_0(\xi/\lambda_G)-K_0(d_G(\theta_0)/\lambda_G)]}\right|. \tag{2.9}$$

In (2.9) the thicknesses d_B, d_G, Fig. 1(a), are constrained by the Read-Shockley formula (1.1):

$$d=d_G+d_B=\frac{b}{\sin\theta}. \tag{2.10}$$

θ_0 is a calibration angle,[2] and ξ is the coherence length evaluated at the temperature of the measurement. In the particular limit where the "bad" superconductor is considerably degraded in comparison to the "good" domain, i.e., when $\lambda_B\gg\lambda_G$, expression (2.9) simplifies further. Since $K_0(z)\approx-\ln(z)$ for $|z|\ll1$,[13] the B-dependent terms in (2.9) can be entirely neglected, which yields the central result

$$\frac{j_c(\theta)}{j_c(\theta_0)}\approx\left|\frac{K_0(\xi/\lambda_G)-K_0(d_G(\theta)/\lambda_G)}{K_0(\xi/\lambda_G)-K_0(d_G(\theta_0)/\lambda_G)}\right|. \tag{2.11}$$

Expressions (2.9)–(2.11) apply equally to any superconductor superlattice and j_c parallel to the superlattice slabs.

Provided λ_G is identified with the host superconductor, expression (2.11) depends just on a single parameter, i.e., $d_G(\theta)$, which must either come from another calculation, such as stress calculations which lead to Eq. (3.1) below, or taken as a fitting parameter. Before discussing this point, it is instructive to examine the structure of (2.11). Note that since $K_0(z)$ diverges as $z\to0$ and since $d_G(\theta)$ decreases as θ increases [Eq. (2.10)] and approaches ξ, there is an angle θ_c when the numerator changes sign and goes negative. The numerator, on the other hand, is proportional to the maximum pinning barrier between the bad and good domains and hence cannot attain a negative sign in a physically viable situation. Consequently, we conclude that at the angle θ_c the London equation (2.1) and ensuing analysis break down. This should be indeed the case since when $d_G(\theta_c)\approx\xi$; i.e., when a characteristic length scale becomes comparable to the coherence length, the macroscopic London approach embodied in (2.1) is supposed to become invalid.

The preceding discussion implies that Eq. (2.11) is valid only for θ angles such that $d_G(\theta)\gtrsim\xi$. In this regime, the structure of (2.11) and the measured rapid θ variation of $j_c(\theta)$ [Ref. 2(b)] imply that $d_G(\theta)$ is considerably larger than $d_B(\theta)$. We arrive at this conclusion as follows: Since $K_0(z)\approx-\ln(z)$ for $|z|\ll1$, the numerator of (2.11) varies rapidly when its two terms approach each other, i.e., when $d_G/\lambda_G\simeq\xi/\lambda_G\ll1$. Consequently, expanding the numerator $K_0(d_G(\theta)/\lambda_G)$ around $K_0(\xi/\lambda_G)$ to first order gives rise to a term proportional to $d_G(\theta)-\xi$. On the other hand, $d_G(\theta)$ is *constrained* by the Read-Shockley formula (2.10), which for small angles is rapidly varying since $\sin(\theta)^{-1}\approx1/\theta$ for $\theta\ll1$. Therefore, provided $d_G(\theta)\gtrsim d_B(\theta)>\xi$ in (2.10), it follows that $d_G(\theta)\approx1/\sin(\theta)$ and (2.11) is compatible with a depen-

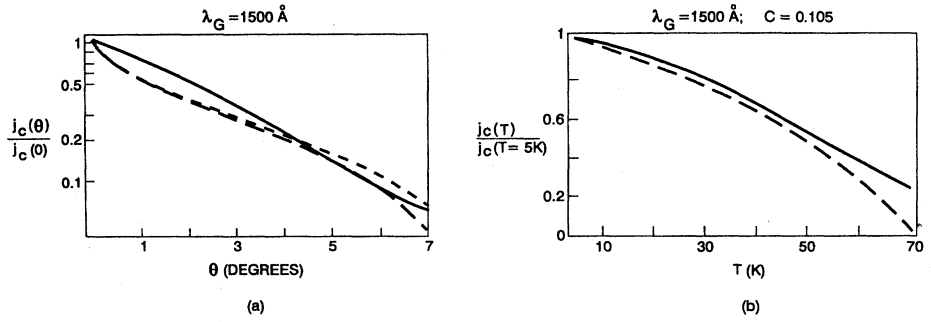

FIG. 4. Comparison of model calculations with data. (a) The $j_c(\theta)/j_c(\theta_0=0.1)$ data at $T=5$ K [Ref. 2(b)] (solid line) and calculated curves employing (2.11) and (3.1), with $C=0.075$ (long-dashed line) and $C=0.105$ (short-dashed line). (b) The $j_c(T,\theta_0)/j_c(T=5\text{ K},\theta_0)$ data at $\theta_0=5°$ [Ref. 2(c)] (solid line) and the calculated curve employing (2.11) and (3.2) (long-dashed line).

dence $j_c(\theta)/j_c(\theta_0)\approx 1/\sin(\theta)$. As shown in the next section, stress-field calculations yield an estimated $d_G(\theta)$ consistent with these considerations. And a particular fit to the data discussed below assumes indeed a $j_c(\theta)\approx 1/\sin(\theta)$ dependence.

III. RESULTS AND DISCUSSION

To apply (2.11) it is necessary to specify $d_G(\theta)$ and the penetration depth λ_G. We identify the good superconductor domain with the Y-Ba-Cu-O host; hence, $\lambda_G(T=4.2\text{ K})\approx 1500$ Å. Given the lack of data or detailed calculations of the dislocation stress field for low-angle GB's, the $d_G(\theta)$ parameter is estimated from stress-field calculations of an edge-dislocation array model outlined in Appendix C.[14–16] The corresponding geometry, depicted in Fig. 1(a), assumes a periodic array of dislocations. From the numerically calculated shear stress field (σ_{xy}), we extract a radius r_0 of an effective circularly stressed domain around each dislocation, Fig. 1(b), by equating the average of $|\sigma_{xy}|$ over the circle to an adjustable value, i.e., $\sigma_c=\langle|\sigma_{xy}|\rangle$. In the vein of the superlattice model, Fig. 1(c), the former is equated to $r_0=d_B/2$. An excellent approximation to the ensuing calculated $d_B(\theta)$ is[14]

$$\frac{d_B(\theta)}{d(\theta)}=0.32\sqrt{\frac{\theta}{C}}, \tag{3.1}$$

where the dimensionless fitting parameter C is $C\approx 2\langle|\sigma_{xy}|\rangle/\mu_m$, with μ_m denoting the classic shear modulus (Appendix C), and $d(\theta)$ is given by the Read-Shockley formula (1.1).

Employing the calculated $d_B(\theta)$ from (3.1) and $d_G(\theta)$ from (2.10), the calculated critical current ratio (2.11) is presented in Fig. 4(a). A good fit with the exponentially decreasing $j_c(\theta)$ data[2(b)] is obtained over the entire range $\theta\leqslant 7°$ for a range of values $C=0.105-0.075$. When compared to an estimate of $\langle|\sigma_{xy}|\rangle/\mu_m$ based on the theoretical shear strength of crystals,[17] which is typically of the order of 1/20–1/30, the above fitted C value is quite reasonable. The corresponding thicknesses, Fig. 5, shows that $d_G(\theta)$ is much larger than $d_B(\theta)$ [which varies as $\theta^{-1/2}$ according to (3.1)] and rapidly drops with θ, closely following that of the periodicity $d(\theta)$ [Eq. (1.1)]. As discussed above, these features are necessary to reproduce the data.

Figure 4(b) shows the calculated temperature dependence of (2.11) and the data.[2(c)] For this calculation we use the "best"-fit parameter $C=0.105$ of Fig. 4(a), which corresponds to the $T=4.2$ K data, fix the misalignment angle at $\theta=5°$, and introduce the standard temperature-dependent penetration length and coherence length[18]

$$\lambda_G(T)\approx\frac{\lambda_G(0)}{\sqrt{1-T/T_c}},\quad \xi(T)\approx\frac{\xi(0)}{\sqrt{1-T/T_c}}, \tag{3.2}$$

with $\xi(0)\approx 15$ Å, $\lambda_G(0)\approx 1500$ Å. As Fig. 4(b) shows, this parameter-free fit is surprisingly good over a wide range of temperatures.

To put our results in perspective, we discuss now the validity of the model and competing models. A major approximation of the present model is the highly simplified superlattice geometry, Fig. 1(c), which supposedly represents the delineation of stress fields associated with the periodic edge-dislocations array, Fig. 1(a). While the geometry of the latter is obviously quite different from that of a superlattice, the resulting good fits to the data of the superlattice model are interpreted to implies that the *rates of change* with θ (or d) of the *ratio* of two j_c [a calibration j_c value and a running j_c; see Eq. (2.11)] for the two geometries are not grossly different. This is attributed to the fact that both geometries satisfy the Read-Shockley formula and entail a periodic structure of two types of domains. In other terms, while the absolute values of the critical currents in the geometries of Figs. 1(a) and 1(c) may be quite different, their *relative rate*

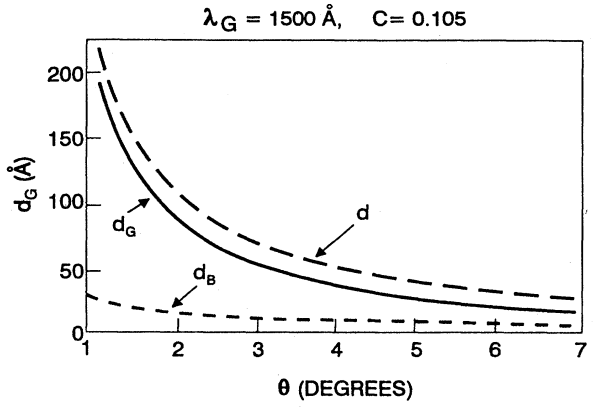

FIG. 5. Superlattice layer thickness θ dependence: The periodicity d, Eq. (1.1) with $b=3.8$ Å [Refs. 2(b), 3], and the "good" (d_G) and "bad" (d_B) layer thicknesses are calculated from Eqs. (2.10), (3.1) with $C=0.105$.

of change with θ, which is the measured quantity, is apparently similar. To check this conjecture quantitatively requires calculations of considerably complexity which are deferred to another publication.

Underlying the model is a transcription of local stress (positive or negative) into a local degradation of superconductivity. This degradation occurs probably through the mechanism of out-diffusion of oxygen atoms and a related change in the carrier concentration as a function of stress.[19] Currently, there is no reliable quantitative model to assess the degree of degradation; therefore, this effect is represented in the present model by a free parameter (λ_B). In the limit of "large" degradation, this ill-defined parameter is entirely eliminated from the final result [Eq. (2.11)], indicating that the key to reproduce the observed data is the length of the superconducting constriction between adjacent dislocations. These observations underscore the importance of stress calculations. Our calculations, Appendix C, employ the shear stress σ_{xy}. Similar results are obtained when the diagonal stress components σ_{xx}, σ_{yy} are employed.[14]

As discussed above, for θ beyond the point where $d_G(\theta) \approx \xi$, the present model breaks down since the dislocation lines get closer than the coherence length and the discrete-dislocation concept loses its validity. For such GB's a more realistic model is to represent them by a continuous slab, which acts either as a Josephson junction weak link[2] or as a nonweak link[20] as observed in some flux-melt ceramics.[5,6]

In all of the above discussion the magnetic field did not enter, corresponding to the experimental setup,[2] which only leads to weak self-fields. This circumstance is consistent with the validity regime of the basic equation (2.1), where the assumed weak field is reflected by an isolated fluxon.

The data under consideration are also the subject of other approaches.[21,22] The model of Ref. 21 produces fits of same data as Fig. 4. It stipulates that the critical current is determined by a combination of an electron-pair tunneling mechanism[23] through a GB effective Josephson junction and a pair-scattering mechanism from charge at the dislocation cores. Using a continuum model for the stresses, the calculated junction effective width for $\theta \leq 7°$ is less than 2 Å. Our difficulties with this model are, first, the assumption that the small angles GB's of Ref. 2 are in effect Josephson junctions. The TEM studies of these GB's (Refs. 2, 3) do not support this premise. Second, given that the Y-Ba-Cu-O coherence length is ≈ 15 Å, it is difficult to justify a tunneling mechanism over a distance ≈ 1 Å. As our analysis demonstrates, the same data can be quantitatively understood in terms of a considerably simpler model. Another attempt at the same data[22(a)] is an empirical fit $j_c(\theta)/j_c(0°) \approx 1/\sin\theta$, reminiscent of the Read-Shockley relation, Eq. (1.1). As discussed at the end of Sec. II, Eq. (2.11) together with the thicknesses calculated in Fig. 5 implies approximately this form of θ behavior when the numerator in (2.11) is expanded to first order. In Ref. 22(b), a configuration of the type depicted in Fig. 1(b) is suggested, however, without any quantitative analysis. As commented above, the corresponding large calculational effort may not be warranted at this point given that the expected outcome will be a data-fitting expression of the type (2.11).

In conclusion, we introduced a superconductor superlattice model and calculated the ensuing critical current ratio measured in small-angle GB's in Y-Ba-Cu-O bicrystals.[2] With a single parameter, which naturally emerges from the pertaining stress-field calculations, the model fits the data small-angle and temperature dependence. The crucial θ dependence enters via the Read-Shockley constraint (1.1) and the estimated layer thicknesses. This model may also be applicable to the analysis of current transport in superconductor superlattices. Such structures, with Y-Ba-Cu-O-like constituents, have been recently fabricated.[24]

APPENDIX A: SOLUTION OF EQ. (2.1)

This appendix provides some details on solving Eq. (2.1) for a piecewise constant, periodic penetration depth profile. All notations and coordinates are defined in Fig. 1(a). The starting point is the homogeneous London equation solutions

$$B_G(x,y) = \int_{-\infty}^{\infty} dk_y e^{ik_y y} [e^{ik_G^{(+)}(k_y)x} B_G^{(+)}(k_y) + e^{ik_G^{(-)}(k_y)x} B_G^{(-)}(k_y)],$$

$$B_B(x,y) = \int_{-\infty}^{\infty} dk_y e^{ik_y y} [e^{ik_B^{(+)}(k_y)x} B_B^{(+)}(k_y) + e^{ik_B^{(-)}(k_y)x} B_B^{(-)}(k_y)],$$

$$k_X^{(\pm)}(k_y) = \pm i D_X(k_y), \quad X = G, B, \tag{A1}$$

where $B_B(x,y)$ and $B_G(x,y)$ denote the fields for $0 \leq x \leq d_B$ and $d_B \leq x \leq d$, respectively.

Inserting the expansion (A1) in Eq. (2.1) yields for a fixed k_y value a one-dimensional wave equation with a periodic potential. According to (2.4), this equation has a complete set of solutions which satisfy the one-dimensional Bloch theorem

$$B_B^{(\pm)}(k_y) = e^{[\mu + ik_G^{(\pm)}(k_y)]d} B_G^{(\pm)}(k_y) \tag{A2}$$

and μ in given by (2.5). The subsequent ratios

$$\frac{B_X^{(\pm)}(k_y,\mu)}{B_X^{(\mp)}(k_y,\mu)}=\beta_X^{(\pm)}(k_y,\mu)\equiv\beta_X^{(\pm)}(\mu),\quad X=G,B, \tag{A3}$$

are given in (2.7b). These ratios determine, up to a k_y-dependent normalization, the solutions (A1).

The solution to Eq. (2.1) is constructed following the standard method for constructing the Green function from a complete set of solutions of the homogeneous equation.[12]

The single-vortex Green function needed in Sec. II is

$$B_B^{(\mathrm{vor})}(x,y)=\frac{\Phi_0}{4\pi\lambda_B^2}\int_{-\infty}^{\infty}dk_y\,\frac{e^{ik_y(y-y_0)-D_B(k_y)(x_>-x_<)}}{D_B(k_y)}=\frac{\Phi_0}{2\pi\lambda_B^2}K_0\left[\frac{\sqrt{(x_>-x_<)^2+(y-y_0)^2}}{\lambda_B}\right]. \tag{A4}$$

APPENDIX B: THE INTEGRAND IN EQ. (2.7a)

To derive the analytical approximation of the pinning potential (2.8), we need the $|k_y|\to 0,\infty$ limits of the integrand in (2.7). To construct these, the approach is to consider first the integrand's "tail," i.e., the $k_y\to\infty$ limit, for which it simplifies and yields the integral representation of the $K_0(z)$; see (A4). Next we consider the $k_y\to 0$ limit, from where the main contribution to the integral (2.7) arises, and relate the two extremes.

In preparation for these steps, Eq. (2.5) yields the following limits of the attenuation factor μ:

$$\mu(0)d=\lim_{k_y\to 0}\mu d=\sqrt{\left(\frac{d_G}{\lambda_G}+\frac{d_B}{\lambda_B}\right)^2+\frac{(1-\rho)^2}{\rho}\frac{d_G d_B}{\lambda_G\lambda_B}},$$

$$\lim_{k_y\to\infty}\mu d=|k_y|d, \tag{B1}$$

where $\rho=\lambda_G/\lambda_B\ll 1$ and we considered the regime where $d_G/\lambda_G, d_B/\lambda_B\ll 1$. The integrand is estimated below at the midpoints of the G and B domains for the reasons given in Sec. II.

Consider first the B domain. Noting that ρ, $\lambda_B/d_B\ll 1$, Eq. (2.7b) yields, for the three terms in (2.7a) at the $|k_y|\to\infty$ limit,

$$\beta_B^{(-)}(\mu>)\beta_B^{(+)}(\mu<)\approx\frac{(1-\rho^2)}{(1+\rho^2)}e^{-2|k_y|d_B},$$

$$e^{-2D_B(k_y)x_0}\beta_B^{(+)}(\mu<)\approx e^{-d_B|k_y|},\quad e^{2D_B(k_y)x_0}\beta_B^{(-)}(\mu>)\approx\frac{1-\rho^2}{1+\rho^2}e^{-|k_y|d_B}, \tag{B2}$$

and the corresponding terms for the $k_y\to 0$ limit are

$$\beta_B^{(-)}(\mu>)\beta_B^{(+)}(\mu<)\approx\frac{(1-\rho^2)}{(1+\rho^2)},$$

$$e^{-2D_B(k_y)x_0}\beta_B^{(+)}(\mu<)\approx\frac{1-\rho^2}{1+\rho^2}e^{d_B/\lambda_B},\quad e^{2D_B(k_y)x_0}\beta_B^{(-)}(\mu>)\approx\frac{1-\rho^2}{1+\rho^2}e^{-d_B/\lambda_B}. \tag{B3}$$

By the same token, the results for the G domain for $|k_y|\to\infty$ are

$$\beta_G^{(-)}(\mu>)\beta_G^{(+)}(\mu<)\approx\frac{(1-\rho^2)}{(1+\rho^2)}e^{-2|k_y|d_G},$$

$$e^{-2D_G(k_y)x_0}\beta_G^{(+)}(\mu>)\approx-\frac{1-\rho^2}{1+\rho^2}e^{-|k_y|d_G},\quad e^{2D_G(k_y)x_0}\beta_G^{(-)}(\mu>)\approx-e^{-|k_y|d_G}, \tag{B4}$$

and for $k_y\to 0$, we get

$$\beta_G^{(-)}(\mu>)\beta_G^{(+)}(\mu<)\approx\left[\frac{(1-\rho^2)}{2}\right]^2\left(\frac{d_B}{\lambda_G}\right)^2 e^{-\mu(0)d-d_G/\lambda_G},$$

$$e^{-2D_G(k_y)x_0}\beta_G^{(+)}(\mu<)\approx-\frac{1-\rho^2}{2}\left(\frac{d_B}{\lambda_G}\right)e^{-\mu(0)d}, \tag{B5}$$

$$e^{2D_G(k_y)x_0}\beta_G^{(-)}(\mu<)\approx-\frac{1-\rho^2}{2}\left(\frac{d_B}{\lambda_G}\right)e^{-d_G/\lambda_G}.$$

The results (B1)–(B5) lead to the key analytical approximation (2.8). To demonstrate this, consider first the B domain. For $k_y\to\infty$, Eq. (B.2) shows that the last two terms are about equal and exponentially large in comparison to the first term (the $\beta\times\beta$ term). These two terms contribute a characteristics tail contribution proportional to $2K_0(d_B/\lambda_B)$; see Eq. (A4). On the other hand, for $k_y\to 0$, Eq. (B3) shows that all three terms in the integrand are about the same. Since most of the contribution to the integral arises from the small k_y domain [see Fig. 3(a)], it is suggestive to approximate the integral for *all* k_y as twice the tail contribution, hence the factor 4 in (2.8). In the G domain, the situation is different. Equation (B4) shows that for large k_y the last two terms are about equal and larger than the first term. Again, they contribute a characteristic tail contribution proportional to $2K_0(d_G/\lambda_G)$. For a small k_y, however, since $\rho=\lambda_G/\lambda_B\ll 1, d_B<d_G$, Eq. (B1) implied that the second term in Eq. (B5) dominates. Therefore it is suggestive to approximate the integrand for all k_y as half the tail contribution, hence the unity factor in (2.8). Although for the very small k_y this approximation overestimates the G-domain integrand [see Fig. 3(b)], it still yields a very good approximation for the integral.

APPENDIX C: STRESS-FIELD CALCULATIONS

The goal is to calculate the radius r_0 of a circular region around each of the dislocation centers, Fig. 1(b), such that the averaged value of the absolute shear stress $|\sigma_{xy}|$ over the circle equals a prescribed value σ_c:

$$\sigma_c=\int_0^{2\pi}d\alpha\,\frac{|\sigma_{xy}(\alpha;r_0)|}{2\pi}=\langle|\sigma_{xy}|\rangle. \tag{C1}$$

In (C1), $x=r_0\cos\alpha$, $y=r_0\sin\alpha$, and the array is along the y axis. The expression for the shear stress of an infinite array of edge dislocations, ignoring core-core interactions is[16]

$$\sigma_{xy}=\frac{\pi\sigma_0 X\mu b[\cosh(2\pi X)\cos(2\pi Y)-1]}{d(1-\nu)[\cosh(2\pi X)-\cos(2\pi Y)]^2}. \tag{C2}$$

$X=x/d$, $Y=Y/d$, ν is the Poisson ratio, μ is elastic shear modulus, b is the Burgers vector, and r_0, d are defined in Fig. 1(b). For small misalignment angles, the Read-Shockley relation gives $d=b/\theta$.

The numerical method for evaluating (C1) utilizes a simple adaptive scheme. Using a least-squares fit and assuming $\nu\approx 1/3$, Eq. (3.1) is obtained, where $C\approx 2\sigma_c/\mu$. Employing the other stress components σ_{xx}, σ_{yy} in (C1) yielded a dependence similar to (3.1).

Equation (C2) is derived from superposition of the stress field of the entire dislocation array, disregarding core-core interactions. To consider the latter, we utilize a simple model,[15] where the radius r_0 is determined by minimizing the total elastic energy which is comprised of the stress-field energy and the core-interface energy. The former is obtained by solving for the stress field in which core-core interaction is introduced via a boundary condition, i.e., imposing a vanishing stress field on and in a circular perimeter around each dislocation of radius r_0, Fig. 1(b). This stress-field energy component favors larger r_0. On the other hand, the total energy component of core-interface energy is proportional to r_0 and pushes for smaller r_0. The r_0 value is obtained by energy minimalization.

Equating the r_0 calculated in this manner with $d_B/2$ and substituting in (2.10), (2.11) gave a considerably worse fit to the data. This outcome can be understood as follows. The qualitative shape of the "correct" stress profile, as function of distance from the dislocation center, follows a rise from zero at the center up to a maximum and then tapers off far from the dislocation center. In the vein of our model, the correct C parameter [Eq. (3.1)] should correspond to an effective r_0 such that it encompasses the highly stressed domain; in particular, r_0 should be *larger* than a typical distance at which the stress profile reached its maximum. The value $0.5C=1/20-1/30$ (Ref. 17) corresponds to such a r_0 choice. On the other hand, in the core-core calculation described above,[15] the circular "core" of radius r_0 is completely unstressed and somewhat larger than the correct value, hence the worse results.

[1] K. A. Muller, M. Takashige, and J. G. Bednorz, Phys. Rev. Lett. **58**, 1143 (1987).

[2] (a) P. Chaudhari, J. Mannhart, D. Dimos, C. C. Tsui, J. Chi, M. M. Oprysko, and M. Schuermann, Phys. Rev. Lett. **60**, 1653 (1988); (b) D. Dimos, P. Chaudhari, J. Mannhart, and F. K. LeGoues, *ibid.* **61**, 219 (1988); (c) D. Dimos, P. Chaudhari, and J. Mannhart, Phys. Rev. B **41**, 4038 (1990).

[3] M. F. Chisholm and D. A. Smith, Philos. Mag. A **59**, 181 (1989).

[4] C. Kittel, *Introduction to Solid State Physics*, 4th ed. (Wiley, New York, 1971), pp. 679–680.

[5] D. C. Larbalestier *et al.*, Physica C **185–189**, 315 (1991); S. E. Babcock, X. Y. Cai, D. L. Kaiser, and D. C. Larbalestier, Nature **347**, 167 (1990).

[6] C. B. Eom, A. F. Marshall, Y. Suzuki, B. Boyer, R. F. W. Pease, and T. H. Geballe, Nature **353**, 544 (1991).

[7] Y. Zhu, Z. L. Wang, and M. Suenaga, Philos. Mag. A (to be published); M. J. Kramer and R. W. McCallum (unpublished).

[8] D. Agassi and J. R. Cullen, Physica C **195**, 277 (1992).

[9] E. T. Whittaker and G. N. Watson, *A Course of Modern Analysis* (Cambridge University Press-Macmillan, New York, 1946), pp. 413–416; N. W. Ashcroft and N. D. Mermin, *Solid State Physics* (Holt, Rinehart and Winston, New York, 1976), Chap. 9.

[10] Z. Radovic, S. Rudojev, and L. Dobrosavljevic, J. Low Temp. Phys. **107**, 107 (1984).

[11] J. P. McKelvey, *Solid State and Semiconductor Physics* (Harper and Row, New York, 1969), pp. 212–217.

[12] P. M. Morse and H. Feshbach, *Methods of Theoretical Physics* (McGraw-Hill, New York, 1953), pp. 825–828.

[13] *Handbook of Mathematical Functions*, edited by M. Abramowitz and I. A. Stegun, Natl. Bur. Stand. Appl. Math. Ser. No. 55 (U.S., GPO, Washington, D.C., 1964), p. 375.

[14] C. S. Pande, R. A. Masumura, and D. Agassi, in *Novel Techniques in Synthesis and Processing of Advanced Materials*, edited by J. Singh and S. M. Copley (TMS, Warrendale, PA, 1994), pp. 67–78.

[15] R. A. Masumura and M. E. Glicksman, Can. Metall. Q. **13**, 43 (1974).

[16] J. P. Hirth and J. Lothe, *Theory of Dislocations*, 2nd ed. (Wiley, New York, 1982), p. 733.

[17] A. H. Cottrell, *Dislocation and Plastic Flow in Crystals* (Oxford University Press, London, 1963), p. 11; J. P. Hirth and J. Lothe, *Theory of Dislocations*, 2nd ed. (Wiley, New York, 1982), p. 7.

[18] M. Tinkham, *Introduction to Superconductivity* (Krieger, Malabar, FL, 1980), p. 113.

[19] D. O. Welch and R. C. Baetzold, in *Advances in Superconductivity V*, edited by Y. Bando and H. Yamauchi (Springer-Verlag, Tokyo, 1993), pp. 37–40.

[20] D. Agassi and R. D. Bardo, J. Electron. Mater. **22**, 1221 (1993).

[21] K. Jagannadham and J. Narayan, Philos. Mag. B **61**, 129 (1990); K. Jagannadham and J. Narayan (unpublished).

[22] (a) T. Matsushita, B. Ni, and K. Yamafuji, Cryogenics **29**, 384 (1989); (b) D. Shi, J. Electron. Mater. **22**, 1211 (1993).

[23] G. Deutscher and K. A. Muller, Phys. Rev. Lett. **59**, 1745 (1987); G. Deutscher, Physica C **153–155**, 15 (1988).

[24] J. Gao *et al.*, Physica C **177**, 384 (1991); C. L. Jia, H. Soltner, G. Jacobs, T. Hahn, H. Adrian, and K. Urban, *ibid.* **210**, 1 (1993); S. Guha, M. Z. Cieplak, S. Valdamannati, C. H. Nien, and P. Lindenfeld, J. Supercond. **7**, 201 (1994); **7**, 181 (1994).